

Full Length Research

Second law analysis of a solar air heater having 60° inclined discrete rib roughness on absorber plate

Thakur Sanjay Kumar^{1*}, Vijay Mittal², N. S. Thakur³ and Anoop Kumar³

¹Department of Mechanical Engineering, BRCM College of Engineering and Technology, Bahal, Bhiwani (Haryana), India.

²Department of Mechanical Engineering, Gateway Institute of Engineering and Technology, Sonipat (Haryana), India.

³Department of Mechanical Engineering, National Institute of Technology, Hamirpur, Himachal Pradesh, India.

Accepted 6 December, 2010

Artificially roughened solar air heaters perform better than the smooth ones under the same operating conditions. However, artificial roughness leads to even more fluid pressure thereby increasing the pumping power. The entropy generation in the duct of solar air heater having 60° inclined discrete rib roughness on one broad wall is studied numerically. The effect of system parameters such as relative roughness height (e/D), relative roughness pitch (P/e) and relative gap position (d/W) have been studied on the heat transfer and entropy generation as well as fluid friction with relative gap width (g/e) 1 and temperature rise parameter ($\frac{\Delta T}{I}$) varied from 0.002 to 0.02. For the range of parameters considers in this study, it is seen that for optimum conditions, the entropy and entropy generation number are minimum with maximum effective efficiency.

Key words: Solar air heater, 60° inclined discrete roughness, entropy generation, effective efficiency.

INTRODUCTION

Flat-plate solar collectors are being used for thermal conversion to raise the temperature of fluid flowing through the collector. Conversion of solar radiations to thermal energy is mainly due to heat transfer coefficient between absorber plate and the fluid flowing in the collector. Several designs of solar air heaters have been developed over the years in order to improve their performance. However, the efficiency of solar air collectors is low because of the low value of the convective heat transfer coefficient between the absorber plate and the air, leading to high absorber plate temperature and greater heat losses to surroundings. Close (1963) discussed solar air heaters for low and moderate temperature applications. It has been found that the main thermal resistance to the heat transfer is due to the formation of a laminar sub-layer on the heat transferring surface, which can be broken by providing artificial roughness on the heat-transferring surface. The artificial roughness has been used extensively for the enhancement of forced convective heat transfer, which

further requires flow at the heat-transferring surface to be turbulent. However, the artificial roughness results in higher frictional losses leading to excessive power requirement for the fluid to flow through the duct. It is therefore, desirable that the turbulence must be created only very close to the surface that is in laminar sub layer only, where the heat exchange take place and the core of the flow is not unduly disturbed to avoid excessive losses. This can be done by keeping the height of the roughness elements small in comparison to the duct dimensions (Gupta et al., 1993). Investigations of solar air heaters that form a system with only one roughened wall and three smooth walls have been carried out by various researchers such as Prasad and Saini (1988), Saini and Saini (1997), Karwa et al. (1999), Bragoria et al. (2002), Jaurker et al. (2006), Karmare and Tikekar (2007), Layek et al. (2007), Varun and Singal (2008), Saini and Verma (2008) and Momin et al. (2002) etc. Studies carried out by these researchers have shown that the geometry of rib, namely shape, pitch, angle of attack and height, affects significantly the heat transfer and friction characteristics of the duct. Lau et al. (1991) investigated the turbulence heat transfer and friction for a fully developed flow in a square duct with inclined

*Corresponding author. E-mail: thakursanjay1973@gmail.com.

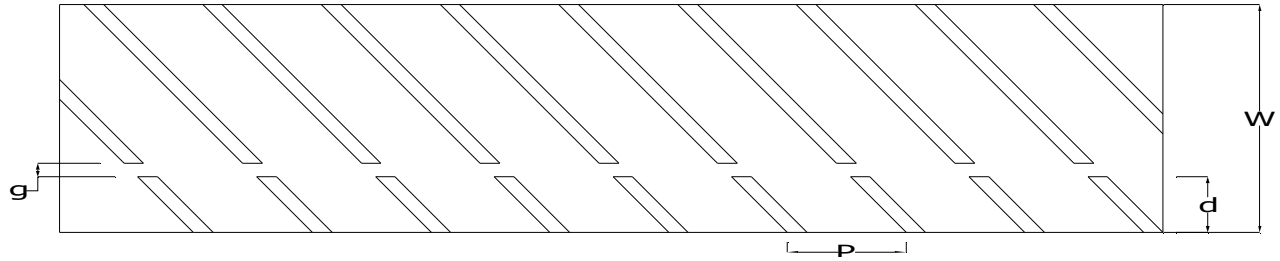


Figure 1. Geometry of 60° inclined discrete rib roughness.

and transverse discrete ribs. The average Stanton number in the 90° discrete rib case is about 10 to 15% higher than that in the 90° transverse rib case. Han and Zhang (1992) investigated the effect of the broken rib orientation on the local heat transfer distribution and pressure drop in a square duct with two opposite roughened walls. The results show that 60° parallel broken ribs or 60° V-shaped broken ribs provide higher heat transfer augmentation than 45° parallel broken or 45° V-shaped broken ribs. Cho et al. (2000) examined the effect of the angle of attack and the number of discrete ribs. The region between the discrete ribs accelerated the flows, and the accelerated flows increased the heat transfer coefficient locally. Cho et al. (2003) investigated the effect of a gap in the inclined ribs on heat transfer in a square duct and reported that a gap in the inclined rib accelerates the flow and enhances the local turbulence, which will result in an increase in the heat transfer. Tanda (2004) investigated heat transfer in rectangular channels with transverse and V-shaped broken ribs with $p/e = 8$ and found that pairs of high heat transfer coefficient lobes are located aside the line normal to ribs (when transverse) or aside the bisector of ribs (when V-shaped). It appears that it will be fruitful to investigate the performance of a solar air heater having absorber plate artificially roughened with optimally 60° inclined discrete rib roughness in order to achieve further enhancement of heat transfer coefficient.

It has been found (Lau et al., 1991; Han and Zhang, 1992; Cho et al., 2000; Cho et al., 2003; Cavallero and Tanda, 2002; Tanda, 2004) that discrete inclined or V-shaped rib arrangement can yield better performance as compared to continuous rib arrangement. Although some studies have examined the performance of rib roughened solar air heater on the basis of first law analysis, to the authors' knowledge, there is rarely study corresponding to performance evaluation of 60° inclined discrete rib roughened solar air heater using second law analysis. The purpose of this paper was to study the effect of various geometrical parameters [relative roughness height (e/D), relative roughness pitch (P/e) and relative gap position (d/W) with relative gap width (g/e) = 1] and flow conditions on the effective efficiency, entropy and entropy generation number of a solar air heater having its absorber plate roughened with 60° inclined discrete rib roughness as shown in Figure 1.

MATHEMATICAL MODELING

Convective heat transfer processes are generally, characterized by two types of losses, namely losses due to fluid friction and those due to heat transfer across a finite temperature difference. Both types of losses are the display of thermodynamic irreversibility. The investigation of a process from this point of view is known as the second law analysis. The second law analysis seeks to minimize these losses in the process by keeping the entropy generation at minimum.

Let us consider the flow passage of cross section, A and the heat transferring surface of width, W shown schematically in Figure 2. The bulk properties of the stream \dot{m} are T_f , P , h , s , ρ . In general, this heat transfer arrangement is characterized by a finite frictional pressure gradient $-\frac{dp}{dx} > 0$ and, when heat is transferred to the stream at a rate q' (W/m), by a finite wall-bulk fluid temperature difference ΔT_m . Considering on a slice of thickness dx as a system, the rate of entropy generation for one inlet and one exit control volume is written as:

$$ds_{gen} = \dot{m}ds - \frac{q'dx}{(T_f + \Delta T_m)} \geq 0 \quad (1)$$

It is also known that if the process is reversible, $ds_{gen} = 0$

and if the process is irreversible, $ds_{gen} > 0$

The first law statement applied to the same system is

$$\dot{m}dh = q'dx \quad (2)$$

Where $q' = \frac{Q_u}{L}$

The second law statement applied to the same system is

$$dh = T_f \times ds + \frac{dP}{\rho} \quad (3)$$

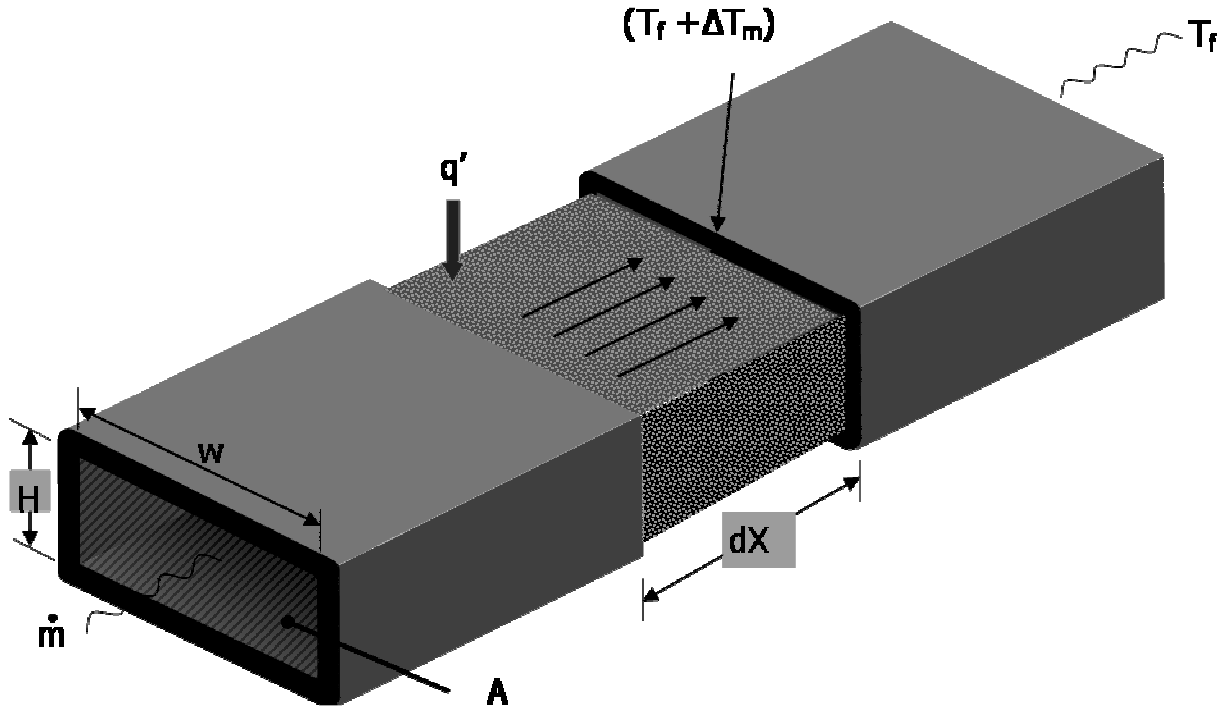


Figure 2. Forced convection heat transfer inside duct of a solar air heater.

Substitution of ds given by Equation (1) and dh given by Equation (2) in Equation (3), gives the entropy generation rate per unit duct length

$$ds'_{gen} = \frac{ds'_{gen}}{dx} = \frac{q'\Delta T_m}{T_f^2(1+\Gamma)} + \frac{\dot{m}}{\rho T_f} \left(-\frac{dP}{dx}\right) \quad (4)$$

In solar air heater, the dimensionless temperature difference $\Gamma = \left(\frac{\Delta T_m}{T_f}\right)$ is negligible compared to unity.

Taken this in to account, Equation (4) reduces to

$$s'_{gen} = \frac{q'\Delta T_m}{T_f^2} + \frac{\dot{m}}{\rho T_f} \left(-\frac{dP}{dx}\right) \quad (5)$$

$$s'_{gen} = s'_{\Delta T} + s'_{\Delta P} \quad (6)$$

Where the first term, $s'_{\Delta T}$, represents the irreversibility due to heat transfer across the wall-fluid temperature difference and the second term, $s'_{\Delta P}$, is the irreversibility caused by fluid friction. In terms of the irreversibility distribution ratio, $\Psi = \frac{s'_{\Delta P}}{s'_{\Delta T}}$ Equation (6) becomes.

$$s'_{gen} = s'_{\Delta T} (1 + \Psi) \quad (7)$$

The relationship between heat transfer q' and wall bulk fluid temperature difference is expressed in terms of Stanton number such as:

$$st = \frac{q'A/W\Delta T_m}{C_p \dot{m}} \quad (8)$$

The fluid friction characteristics of a certain duct are usually reported in the form of friction factor correlations:

$$f = \frac{\rho DA^2}{2\dot{m}^2} \left(-\frac{dP}{dx}\right) \quad (9)$$

Considering the case where the heat transfer rate, q' and mass flow rate, \dot{m} are specified. The dependence of s'_{gen} on Stanton number and friction factor is written as:

$$s'_{gen} = \frac{q'^2 H}{T_f^2 C_p \dot{m} st} + f \frac{2\dot{m}^3}{\rho^2 T_f DA^2} \quad (10)$$

$$\Psi = 2 \left(\frac{f}{Dst}\right) \left(\frac{T_f}{\Delta T_m}\right)^2 \left(\frac{\dot{m}^2}{\rho^2 T_f AWC_p}\right) \quad (11)$$

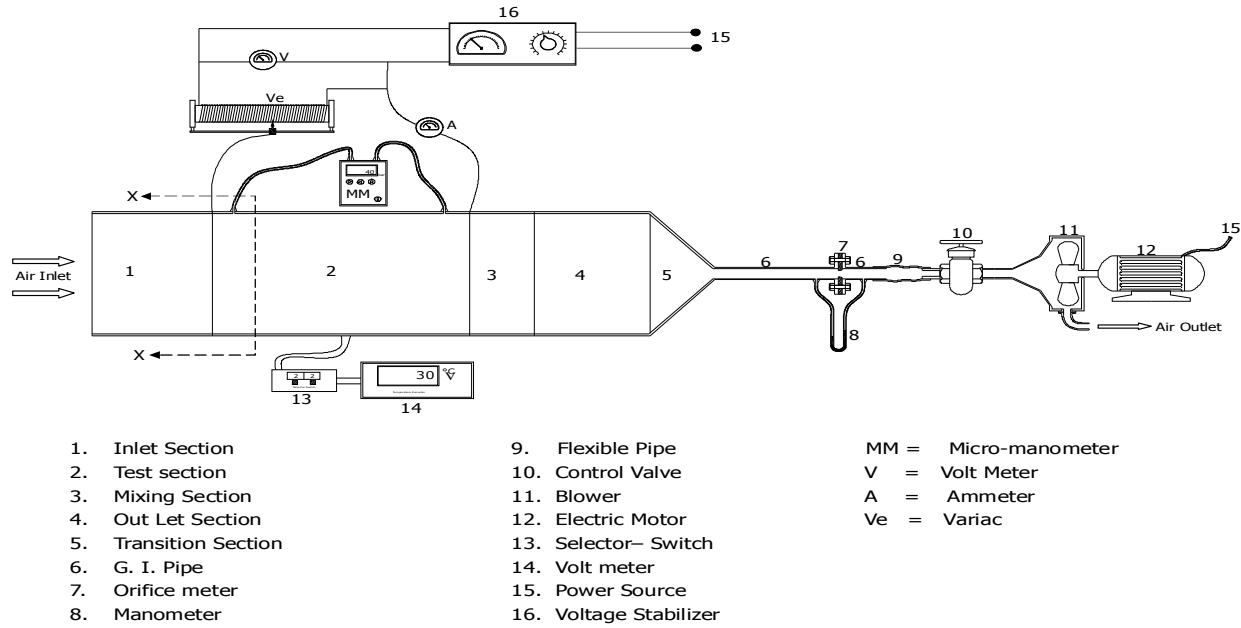


Figure 3. Schematic diagram of experimental set-up.

The impact of an augmentation technique on the irreversibility of a known solar air heater can be evaluated directly by calculating the entropy generation rate in the augmented passage, $s'_{gen,a}$ and comparing it with the entropy generation rate in the unaugmented passage, $s'_{gen,o}$.

To quantize the thermodynamic impact of the augmentation technique, Bejan (1982) defined the augmentation entropy generation number

$$N_{s,a} = \frac{s'_{gen,a}}{s'_{gen,o}} = \frac{(1 + \Psi_a) s'_{a,\Delta T}}{(1 + \Psi_o) s'_{o,\Delta T}} \quad (12)$$

Suffix 'a' for augmented surface and 'o' for smooth surface.

Augmentation techniques with $N_{s,a} < 1$ are thermodynamically advantageous since in addition to enhancing heat transfer they also reduce the degree of the irreversibility of the apparatus. Since the absorber plate roughness has a negligible impact on the flow cross-section area and hydraulic diameter. It is easy to show that when l , $\Delta T/l$, T_i and T_o are the same for smooth and augmented absorber plate of solar air heater, the entropy generation number can be written as:

$$N_{s,a} = \left(\frac{1 + \Psi_a}{1 + \Psi_o} \right) \times \left(\frac{st_a \times R_{ea}}{st_o \times R_{eo}} \right) \times \left(\frac{\Delta T_{ma}}{\Delta T_{mo}} \right) \quad (13)$$

Cortes and Piacentini (1990) defined the effective efficiency (η_{eff}) of solar air heater as the ratio of the net energy gain to the energy available as insolation. The net energy gain is obtained by subtracting the pumping power from the energy gained by the air flowing through the collector. Thus, the effective efficiency represents the net gain per unit solar energy input. It is expressed as:

$$\eta_{eff} = \frac{Q_{u1} - P/C}{IA_p} \quad (14)$$

Where C is conversion efficiency (mechanical power to thermal). Considering that mechanical power is obtained from a typical thermal power plant. The value of C is taken by considering typical values of various efficiencies as 0.2 [=thermal power plant efficiency (0.34) × transmission efficiency (0.90) × motor efficiency (0.90) × efficiency of the pump (0.75)]

EXPERIMENTAL SET-UP AND DATA REDUCTION

The experimental setup is an open loop flow system has been designed and fabricated to conduct experimental investigation on the heat transfer and fluid flow characteristics of a rectangular duct having 60° inclined discrete ribs roughness on the heated surface. The experimental data collected are to be used to develop correlations for heat transfer coefficient and friction factor. Figure 3 is a schematic diagram of the indoor

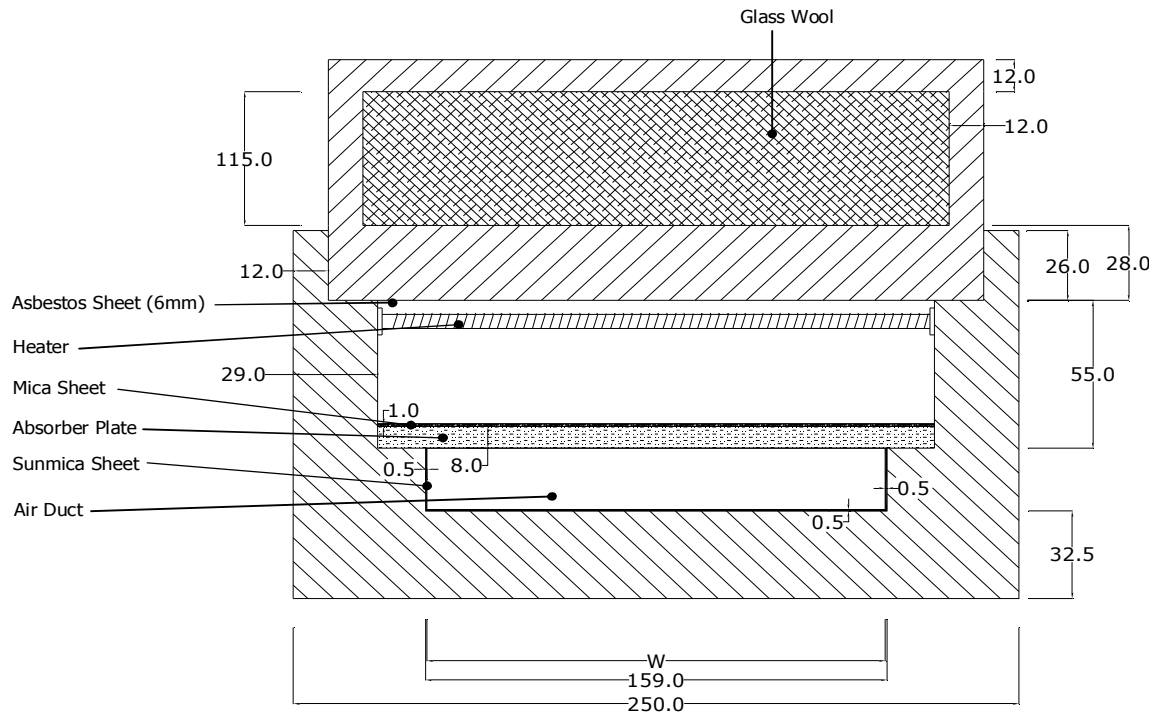


Figure 4. Cross sectional details of test section.

experimental setup including test section. The experimental setup consists of a test duct along with entrance and exit sections, a blower and control valves, a calibrated orifice plate and various devices for measurement of pressure and temperature drop. The blower sucks atmospheric air through the duct, having artificial roughness produced by fixing 60° inclined discrete ribs on the underside of the top plate. The flow through the duct can be controlled by means of control valves provided on the line. Mass flow rate of air was measured by means of an orifice meter on the suction side and connected to an inclined manometer. The wooden rectangular duct has internal size as $2200 \times 158 \times 23$ mm depicting an aspect ratio of 6.9 as shown in Figure 4. It is constructed from wood. The test section has a length of 1000 mm with a cross section of 158×23 mm. It consists of an entrance section, a test section and an exit section having lengths as 550, 1000 and 650 mm respectively. It may be noted that for turbulent flow regime, ASHRAE Standard (1950: 93-77) recommends entry and exit lengths as $5 \sqrt{W \times H}$ and $2.5 \sqrt{W \times H}$ respectively, which has been used in designing the duct for this experimental work. In the exit section three equally spaced baffles are provided after the test section at each 75 mm lengths for the purpose of mixing the delivered air.

At the end of duct a plenum was provided to connect the rectangular duct with circular pipe. An aluminium plate $1000 \times 158 \times 8$ mm is used as artificially roughened plate at the test section of the duct. The artificial

roughness was produced by pasting the aluminium wires on to the underside. The diameter of wire has been varied to get different heights of roughness. This plate is heated from the top by means of an electric heater assembly and is subjected to uniform heat flux. An electric heater having a size of 1000×158 mm was fabricated by combining series and parallel loops of resistance heating wire fitted on 5 mm asbestos sheet. The back side of the heater was insulated with glass wool, to minimize thermal energy losses. The heater placed 42 mm above the roughened absorber plate with the help of wooden spacers. A mica sheet of 0.5 mm thickness is provided between the electric heater and the roughened aluminium plate to avoid the direct contact between heater coil and absorber plate. Energy input to the heater was controlled by a variac so that desired levels of heat flux values could be attained. Ambient air was sucked through the duct system by means of a centrifugal blower driven by a 3-phase, 5 HP, 230 V and 2880 rpm motor. The blower is used to suck the ambient air through the rectangular duct using pipelines and delivered to atmosphere. The air flow rate is regulated at desired rate by providing two control valves, one on the inlet side and other on the outlet side of blower. The mass flow rate of air through duct is measured by orifice meter, which is calibrated for flow rate measurement by experimentally measuring orifice meter co-efficient (C_d) as proposed by Scott et al. (2002) and an average value of C_d can be taken as 0.61. Copper-constantan thermocouples were used for air and absorber plate

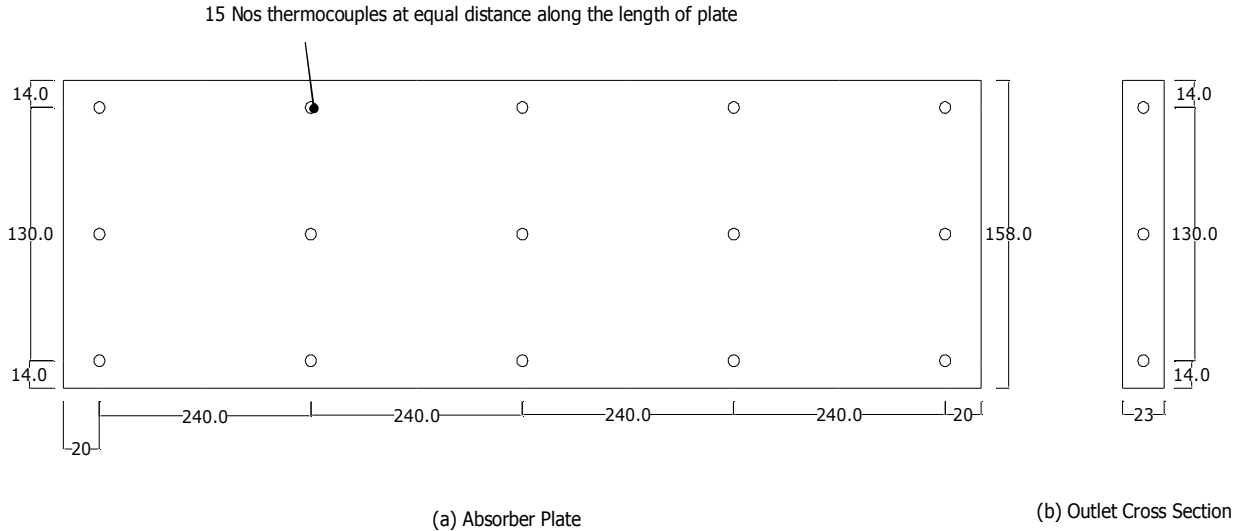


Figure 5. Location of thermocouples on absorber plate and outlet section of the duct.

temperature measurements as shown in Figure 5. Before installing the thermocouples in place, they were calibrated under similar environmental conditions. Fifteen have been fixed using fast drying epoxy resin, through 2 mm deep hole of 1.5 mm diameter at the back of the plate. After the mixing section, three thermocouples arranged transverse of the duct to measure the exit air temperature. All thermocouples were connected to digital voltmeter through a selector switch so that the output could be measured in millivolt (mV) and converted into °C with the help of mV versus °C chart for Copper-constantan thermocouple. The bulk temperature of the entrance section is measured by providing one thermocouples at the entrance section. The pressure drop across the test section of the duct was measured by means of a micro-manometer having a least count of 0.01 mm.

The micro manometer consists of a movable reservoir, a fixed reservoir and an inclined transparent tube connected to these reservoirs. An air bubble is trapped by means of a hypodermic needle. The movable reservoir is mounted on a sliding arrangement using a lead screw having a pitch of 1.0 mm and a graduated dial having 100 divisions; each division showing a movement of 0.01 mm of the reservoir. The movable reservoir is displaced up or down to maintain the air bubble at the specified location for any pressure difference between the two reservoirs and the movement of the moving reservoir is noted as the pressure difference across the two pressure tapings connected to the reservoirs.

Before starting any experiments, all the thermocouples were checked carefully so as to indicate the room temperature and all the pressure tapings were checked for air leakage, if any. The micro manometer and the inclined U – tube manometer were properly leveled. After proper checking of instruments, the test setup was

checked and readied for conducting experiments. The power supply to the centrifugal blower and the electric heater was switched on and the desired flow rate was set with the help of control valves. The steady state condition is assumed to have been reached when the temperature at any point does not change for 10 min. When a change in the operating conditions is made, it takes about 30 min to reach the steady state again. Six values of flow rates were employed for each set of test using constant value of heat flux during the test. After each change of flow rate, the system is allowed to attain the steady state before the data were recorded. The following parameters were recorded.

- i. Pressure difference across the orifice meter.
- ii. Pressure drop across the test section.
- iii. Temperature of the absorber plate.
- iv. Temperature of air at inlet and outlet of the test section.

Steady state values of the plate and air temperatures in the duct at various locations were used to determine the values of useful parameters, namely mass flow rate " \dot{m} ", heat supplied to the air " Q_u " and heat transfer coefficient " h " calculated as:

$$\dot{m} = C_d \times A_o \times \left[\frac{2 \cdot \rho \cdot (\Delta P)_o}{1 - \beta^4} \right]^{0.5} \tag{15}$$

Where $(\Delta P)_o = 9.81 \times (\Delta h)_o \times \rho_m \times \sin \theta$

$$Q_u = \dot{m} C_p (T_o - T_i) \tag{16}$$

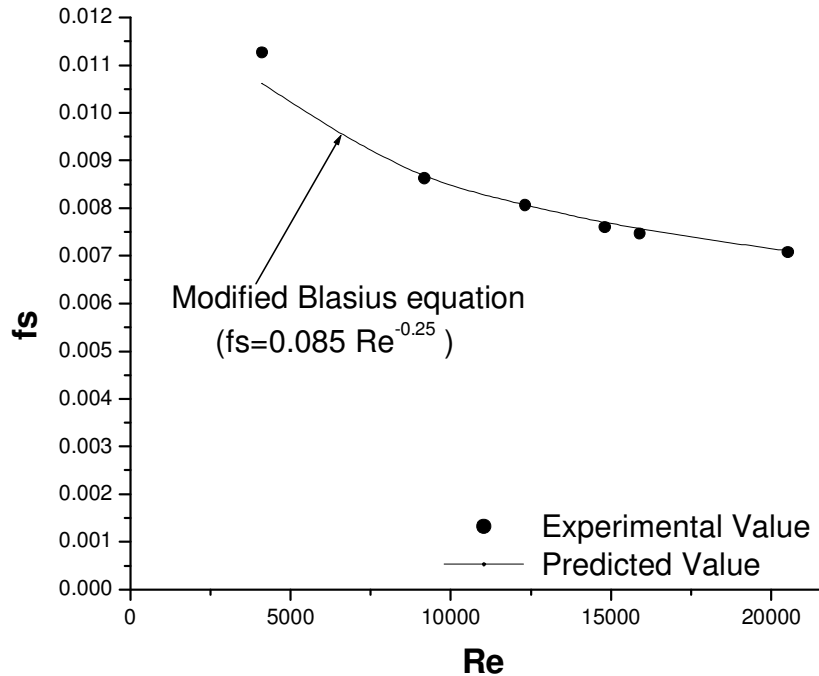


Figure 6. Friction factor vs. Reynolds number for smooth duct.

$$h = \frac{Q_u}{A_p(T_p - T_f)} \quad (17)$$

Where the temperature T_p and T_f are average temperature values of absorber plate and fluid respectively. The average value of plate temperature (T_p) was determined from the detailed temperature profile of the absorber plate indicated by 15 thermocouples at various locations. The convective heat transfer coefficient was then used to obtain Nusselt number, Nu as:

$$Nu = \frac{hD}{K} \quad (18)$$

The friction factor was determined from the measured values of pressure drop, $(\Delta P)_d$, across the test section length, between the two points located 1 m apart.

$$f = \frac{2(\Delta P)_d D}{4\rho L V^2} \quad (19)$$

Where, $(\Delta P)_d = 9.81 \times (\Delta h)_d \times \rho_m$

It may be noted that prior to actual data collected, the test setup was checked by conducting experiments for a

smooth duct. The Nusselt number and friction factor determined from these experimental data were compared with the values obtained from the correlations that is Dittus-Blasius equation for friction factor (Bhatti and Shah, 1987) and Dittus-Boelter equation for Nusselt number (Kays, 1996) in case of smooth duct. These equations are given below:

Blasius equation:

$$f_s = 0.085 \times Re^{-0.25} \quad (20)$$

Dittus-Boelter equation:

$$Nu_s = 0.024 \times Re^{0.8} \times Pr^{0.4} \quad (21)$$

The comparison of measured and predicted values of friction factor and Nusselt number are shown in Figures 6 and 7 respectively. The agreement is seen to be reasonably good. The above comparison ensures the accuracy of experimental results proposed to be obtained from the present experimental set up and instrumentation.

CORRELATION FOR NUSSELT NUMBER AND FRICTION FACTOR

The statistical correlations are developed here to cover total 162 experimental data corresponding to all the twenty seven roughened absorber plates. Regression analysis is carried out to find a relationship that yields a best fit equation for Nusselt number and friction factor.

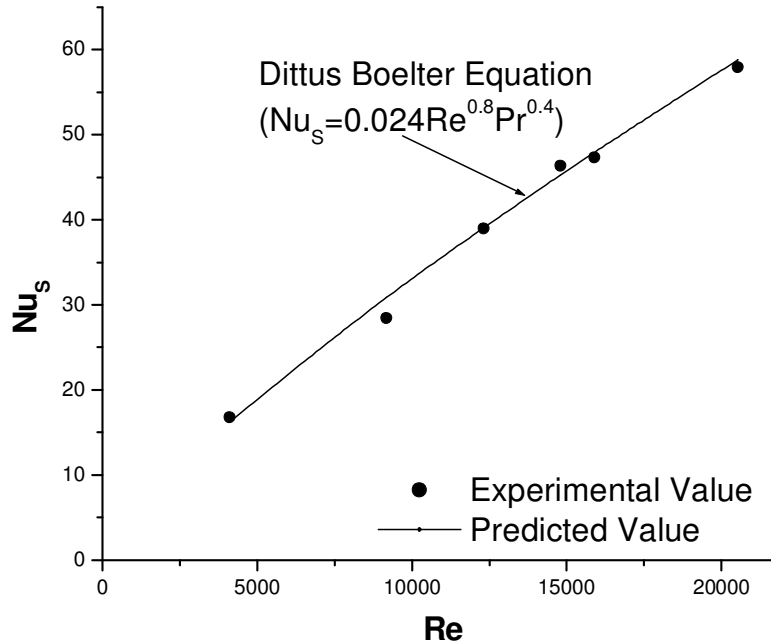


Figure 7. Nusselt number vs. Reynolds number for smooth duct.

The Nusselt number and friction factor depends strongly on roughness parameters, e/D , P/e , d/W and the operating parameter, Re . Thus the equation for Nusselt number and friction factor can be written as:

$$Nu = Nu (Re, e/D, P/e, d/W) \tag{22}$$

$$f = f (Re, e/D, P/e, d/W) \tag{23}$$

The final correlations for Nusselt number and friction factor can be written in the following form,

$$Nu = 3 \times 10^{-5} (Re)^{0.947} (e/D)^{0.290} (P/e)^{5.885} (d/W)^{0.115} \times \exp^{-1.237 (\ln(P/e))^2} \tag{24}$$

$$f = 0.014 Re^{-0.23} (e/d)^{0.804} (d/W)^{0.097} (P/e)^{4.516} \times \exp^{-0.944 (\ln(P/e))^2} \tag{25}$$

These correlations are being used to perform the thermodynamic analysis on solar air heater.

Figure 8 shows a comparison between the experimental values of Nusselt number and those predicted from the correlation developed in Equation 24, around 94% (153 out of 162) of the data points are observed to lie within $\pm 9\%$. The standard deviation is $\pm 4.46\%$. It is therefore concluded that the above heat transfer correlation is reasonably satisfactory. Figure 9 shows the comparison between the experimental values of friction factor and those predicted by the respective correlating Equation (25). The ninety five percent of data points lie within $\pm 9\%$ (155 out of 162). The standard deviation is \pm

5.48%. It is found that the correlation predicts the values of friction factors reasonably well in the range of parameters investigated.

METHOD OF COMPUTATION

The thermal behavior of artificially roughened solar air heater is similar to that of usual flat plate conventional air heater; the usual procedures of calculating the absorbed irradiation and the heat losses can be used. More over the range of operating parameters for conducting the experiments are also given in Table 1. The most important assumptions and simplifications which have been used are:

- i. Steady-state conditions;
- ii. Heat conduction in flow direction neglected;
- iii. Edge effects neglected; constant air flow throughout the collector;
- iv. Sky treated as black body with a temperature equal to the ambient temperature.

Experimental investigations to determine Nusselt number and friction factor depending on the geometrical parameters have been done by the authors; these correlations are used in this paper for the numerical analysis.

The thermodynamic analysis of a solar air heater can also be predicted on the basis of detailed consideration of heat transfer processes in the system. This study is performed for different cases of artificial roughness surfaces on absorber plates of solar air heaters. Using

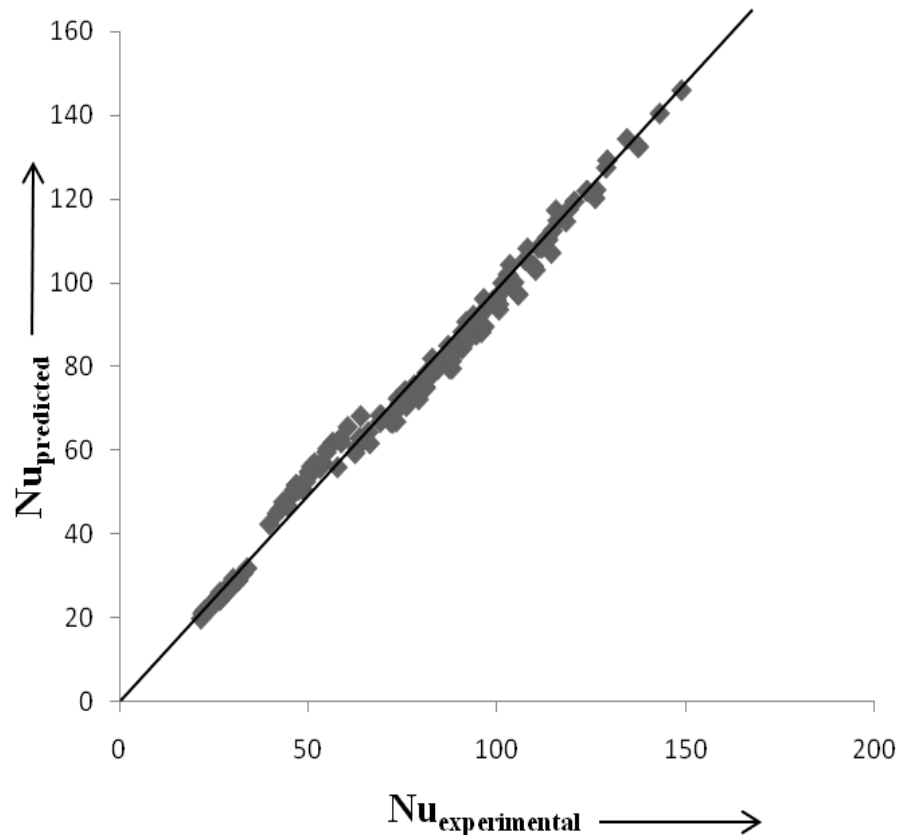


Figure 8. Comparison of Nusselt number for experimental values with predicted values.

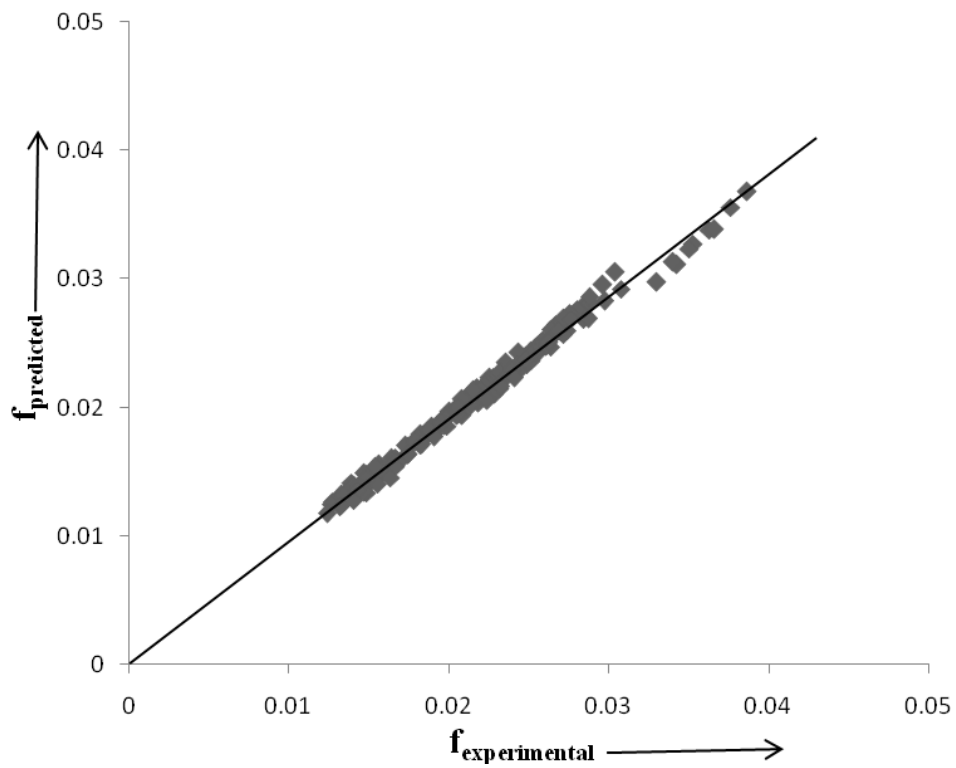


Figure 9. Comparison of friction factor for experimental values with predicted values.

the correlations for Nusselt number and friction factor developed as given in Equations (24) and (25), and the performance parameters, namely overall heat transfer coefficient, heat removal factor and other relevant factors can then be evaluated. For this purpose a step-by-step procedure has to be followed. Various steps involved in the calculation have been explained below. Area of absorber plate is given as:

$$A_p = W \times L \quad (26)$$

Hydraulic diameter of duct as given below

$$D = \frac{2WH}{(W + H)} \quad (27)$$

$$\Delta T = \frac{\Delta T}{I} \times I \quad (28)$$

$$T_o = T_i + \Delta T \quad (29)$$

The mean bulk air temperature

$$T_f = \frac{(T_i + T_o)}{2} \quad (30)$$

The specific heat of air, $C_p = 1006 \left(\frac{T_f}{293} \right)^{0.0155}$ (31)

The dynamic viscosity of air, $\mu = 1.81 \times 10^{-5} \left(\frac{T_f}{293} \right)^{0.735}$ (32)

The thermal conductivity of air, $K = 0.0257 \times \left(\frac{T_f}{293} \right)^{0.8}$ (33)

The density of air, $\rho = \frac{97500}{287.045 \times T_f}$ (34)

The Prandtl number of air is given as:

$$Pr = \frac{\mu \times C_p}{K} \quad (35)$$

The bottom heat loss coefficient

$$U_b = \frac{k_i}{t_i} \quad (36)$$

The edge heat loss coefficient is given below:

$$U_e = \frac{(W + L) \times L_1 \times k_i}{W \times L \times t_e} \quad (37)$$

An initial for the mean absorber plate temperature T_p is made by using the approximation

$$T_p = T_a = T_i$$

The top loss coefficient U_t can be computed by using the relation proposed by Klien (1975)

$$U_t = \left[\frac{N}{\frac{c_t}{T_p} \left(\frac{T_p - T_a}{N + f_t} \right)^{0.33} + \frac{1}{h_w}} \right]^{-1} + \left[\frac{\sigma(T_p^2 + T_a^2)(T_p - T_a)}{1 + \frac{2 \times N + f_t - 1}{\epsilon_g}} \right] \quad (38)$$

Where

$$h_w = 5.7 + 3.8 \times V_w \quad (39)$$

$$c_t = 365.9 \left[1 - 0.00883 \times S + 0.0001298 \times S^2 \right] \quad (40)$$

$$f_t = \left(1 + 0.04 \times h_w + 0.0005 \times h_w^2 \right) (1 + 0.091 \times N) \quad (41)$$

The overall heat loss coefficient is calculated as:

$$U_L = (U_b + U_e + U_t) \quad (42)$$

The useful heat gain is calculated as:

$$Q_{ul} = [I(\Gamma\alpha) - U_L(T_p - T_a)] \times A_p \quad (43)$$

The mass flow rate is calculated as:

$$\dot{m} = \frac{Q_{ul}}{C_p \times \Delta T} \quad (44)$$

The Reynolds number for the flow of air in the duct is computed as:

$$R_e = \frac{G_o \times D}{\mu} \quad (45)$$

Where $G_o = \frac{\dot{m}}{W \times H}$

The Nusselt number calculated using the correlation

Table 1. Typical values of system and operating parameters.

Parameters	Values
Length, L	1000 mm
Width, W	158 mm
Height, H	23 mm
Insolation, I	1075 W/m ²
Transmittance-absorptance, $\tau\alpha$	0.8
Emissance of glass, \mathcal{E}_g	0.88
Emissance of plate, \mathcal{E}_p	0.9
Temperature rise parameter, $\Delta T / I$	0.002 – 0.02 K m ² /W
Relative roughness pitch, p/e	8,12,16
Relative roughness height, e/D	0.0249,0.0311,0.0374,0.436, 0.0498
Relative gap position, d/W	0.15,0.2,0.25,0.3,0.35
Relative gap width, g/e	1

given in Equation 24. The convective heat transfer coefficient is calculated as:

$$h = \frac{N_u \times K}{D} \quad (46)$$

The collector efficiency factor is then determined as:

$$F_p = \frac{h}{h + U_L} \quad (47)$$

The heat removal factor is calculated as:

$$F_o = \frac{\dot{m} \times C_p}{A_p \times U_L} \left[1 - \exp\left(-\frac{A_p U_L F_p}{\dot{m} C_p}\right) \right] \quad (48)$$

The useful heat gain is computed as:

$$Q_{u2} = F_o \times A_p [I(\Gamma\alpha) - U_L(T_o - T_i)] \quad (49)$$

The value of Q_{u1} and Q_{u2} are compared. Ideally the two values should be same. If the difference is more than the 0.1% of Q_{u1} , then plate temperature is modified as:

$$T_p = T_a + \left[\frac{\left\{ I(\Gamma\alpha) - \frac{Q_{u2}}{A_p} \right\}}{U_L} \right] \quad (50)$$

Using the new plate temperature, the calculation from

Equations 38 to 49 are performed again till the difference between the two values of useful heat gain that is Q_{u1} and Q_{u2} is reduced to a value below 0.1% of Q_{u1} . The thermal efficiency is given as:

$$\eta_{th} = \frac{Q_{u1}}{I \times A_p} \quad (51)$$

The friction factor is calculated from the correlation given in Equation 25. The pressure drop in the duct is computed as:

$$\Delta P = \frac{4fL\rho V^2}{2D} \quad (52)$$

$$P = \frac{\dot{m} \times \Delta P}{\rho} \quad (53)$$

$$\Delta T_m = T_p - T_f \quad (54)$$

RESULTS AND DISCUSSION

The procedure describe in articles 2 and 5 has been used to calculate the effective efficiency, entropy and entropy generation number of solar air heater ducts having 60° inclined discrete ribs artificial roughness. These calculations have been carried out for a set of operating parameters as given in Table 1.

Figures 10, 11 and 12 show the effective efficiency, entropy and entropy generation rate, as a function of temperature rise parameter and relative roughness pitch for relative roughness height of 0.0498 and relative gap

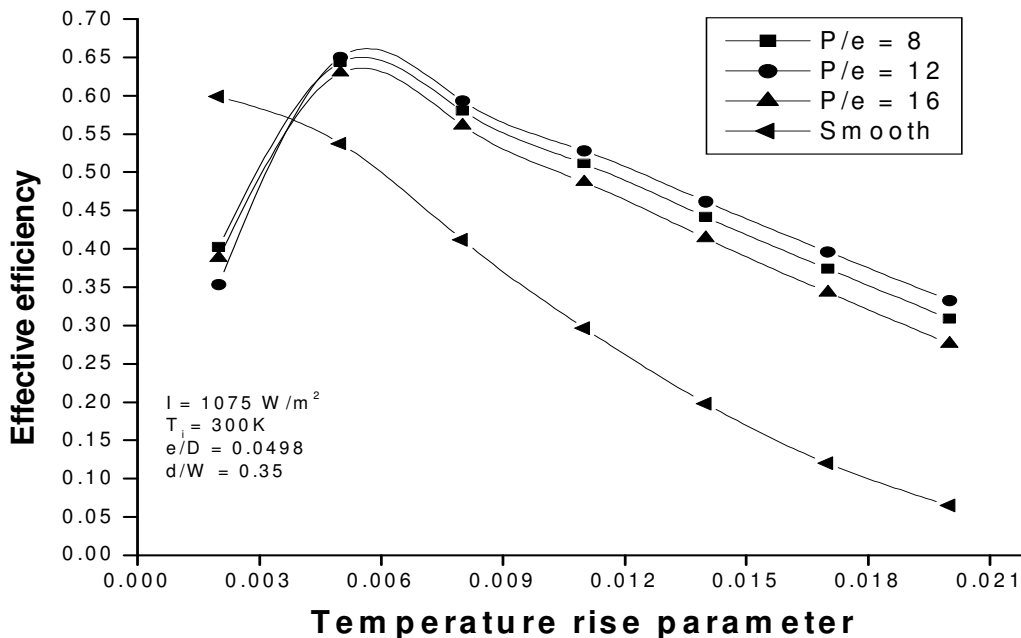


Figure 10. Effective efficiency Vs temperature rise parameter for $e/D=0.0498$ and $d/W=0.35$.

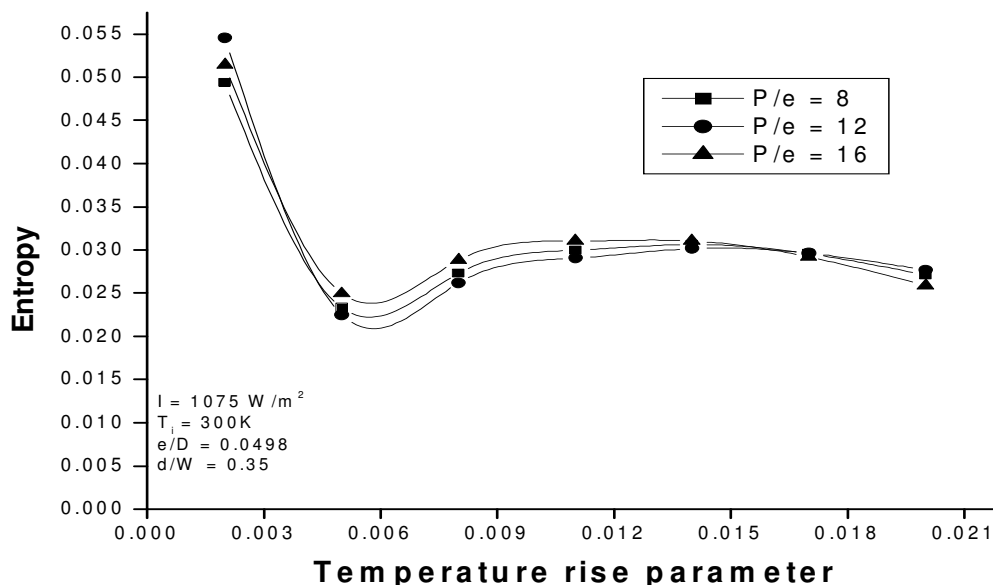


Figure 11. Entropy Vs temperature rise parameter for $e/D=0.0498$ and $d/W=0.35$.

position of 0.35. Figure 10 shows effective efficiency for three values of (P/e) and one for smooth absorber plate. For the temperature rise parameter lower than $0.038 \text{ K/m}^2\text{W}$ smooth absorber plate gives the best performance and relative roughness pitch of 12 has minimum value of effective efficiency. For the temperature rise parameter higher than $0.038 \text{ K/m}^2\text{W}$ relative roughness pitch of 12 has the best performance compared to relative roughness pitches of 8 and 16 and smooth absorber plate gives minimum value of effective

efficiency. Figure 11 depicts the effect of relative roughness pitch on the entropy for relative roughness height of 0.0498 and relative gap position of 0.35. For the temperature rise parameter lower than $0.044 \text{ K/m}^2\text{W}$ relative roughness pitch of 8 has minimum value of entropy. For the temperature rise parameter between $0.044 \text{ K/m}^2\text{W}$ to $0.016 \text{ K/m}^2\text{W}$ relative roughness pitches of 12 has minimum entropy. For the temperature rise parameter higher than $0.016 \text{ K/m}^2\text{W}$ relative roughness pitch of 16 has the best performance, that is, minimum

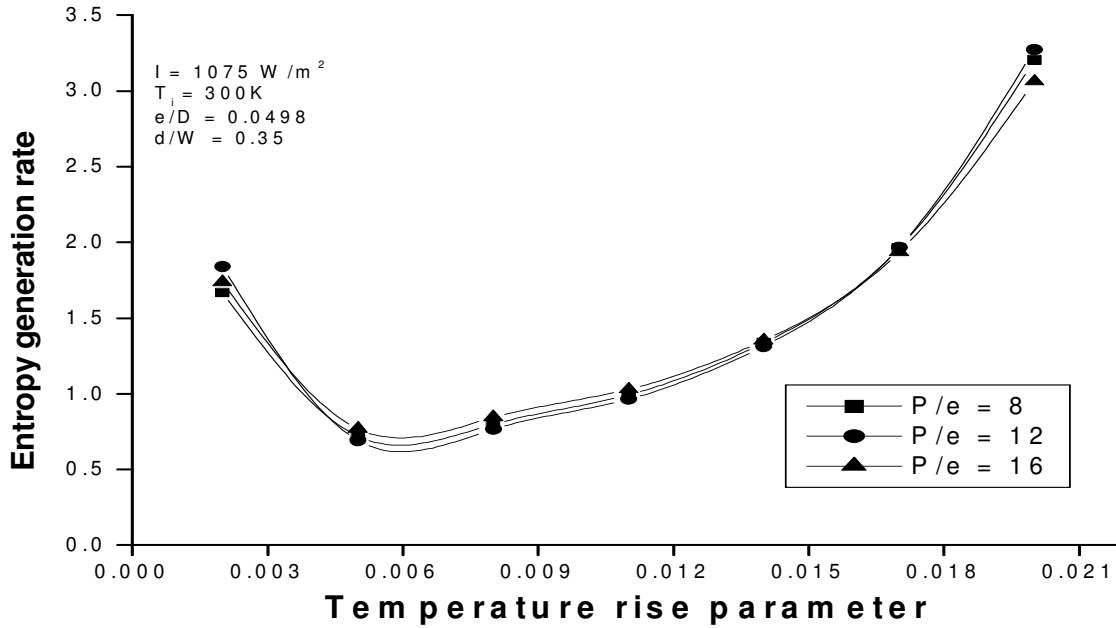


Figure 12. Entropy generation number Vs temperature rise parameter for $e/D= 0.0498$ and $d/W=0.35$.

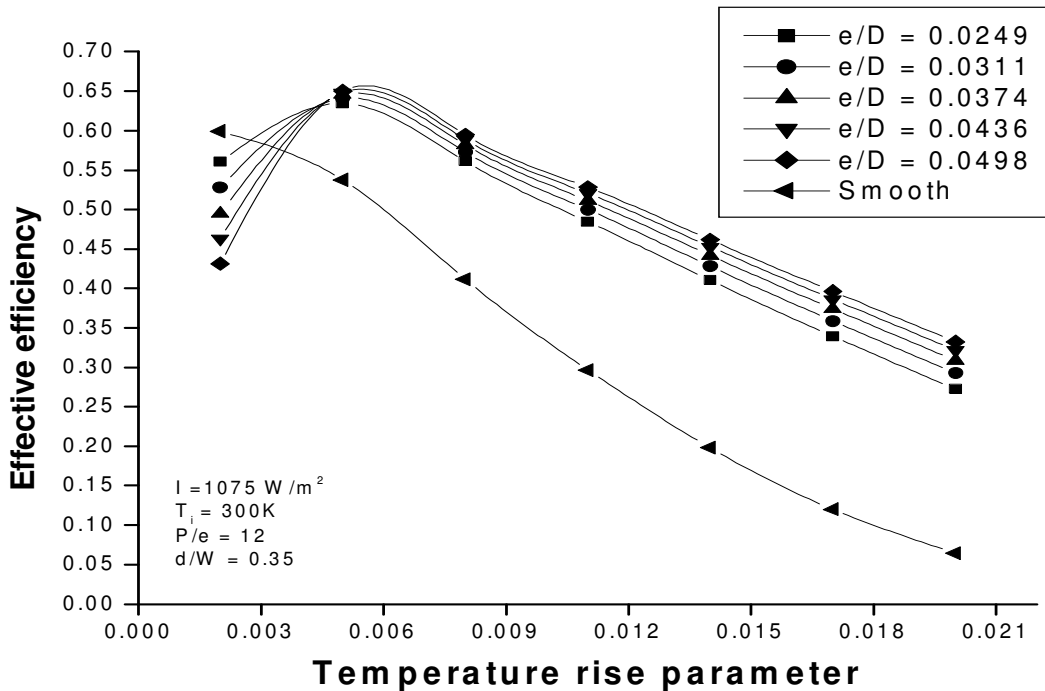


Figure 13. Effective efficiency Vs temperature rise parameter for $P/e= 12$ and $d/W=0.35$.

value of entropy. Figure 12 depicts the effect of relative roughness pitch on the entropy generation number for relative roughness height of 0.0498 and relative gap position of 0.35. For the temperature rise parameter lower than 0.044 $\text{K/m}^2\text{W}$ relative roughnesses pitch of 8 has minimum value of entropy generation number. For

the temperature rise parameter between 0.044 $\text{K/m}^2\text{W}$ to 0.016 $\text{K/m}^2\text{W}$ relative roughness pitch of 12 has minimum entropy generation number. For the temperature rise parameter higher than 0.016 $\text{K/m}^2\text{W}$ relative roughness pitch of 16 has minimum entropy generation number. Figures 13, 14 and 15 show the effective efficiency,

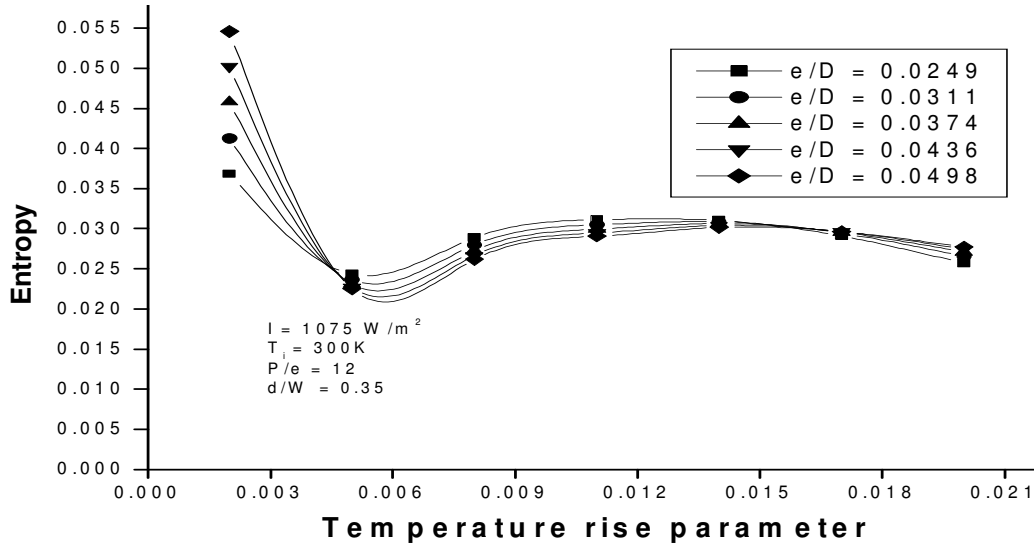


Figure 14. Entropy Vs temperature rise parameter for P/e= 12 and d/W=0.35.

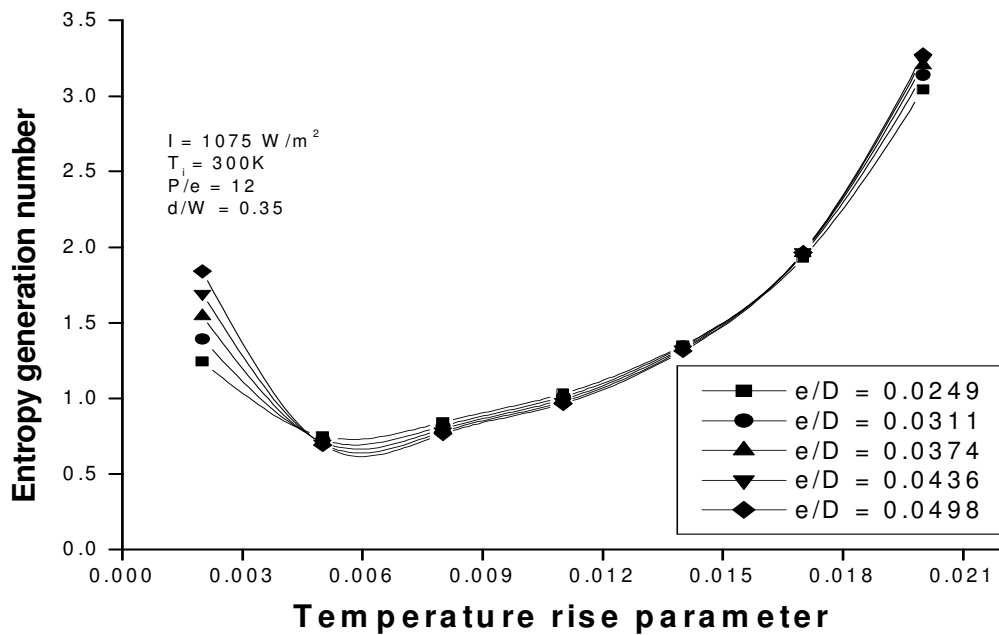


Figure 15. Entropy generation number Vs temperature rise parameter for P/e= 12 and d/W=0.35.

entropy and entropy generation rate, as a function of temperature rise parameter and relative roughness height for relative roughness pitch of 12 and relative gap position of 0.35. Figure 13 shows effective efficiency for five values of (e/D) and one for smooth absorber plate. For the temperature rise parameter lower than 0.038 K/m²W smooth absorber plate gives the best performance. For the temperature rise parameter higher than 0.038 K/m²W relative roughness height of 0.0498 has the best performance height for relative roughness pitch of 12 and relative gap position of 0.35. Figure 14

depicts the effect of relative roughness height on the entropy for relative roughness pitch of 12 and relative gap position of 0.35. For the temperature rise parameter lower than 0.044 K/m²W relative roughness height of 0.0249 has minimum entropy. For the temperature rise parameter between 0.044 to 0.016 K/m²W relative roughness height of 0.0498 has minimum entropy. For the temperature rise parameter higher than 0.016 K/m²W relative roughness height of 0.0249 has minimum entropy. Figure 15 depicts the effect of relative roughness height on the entropy generation number for relative

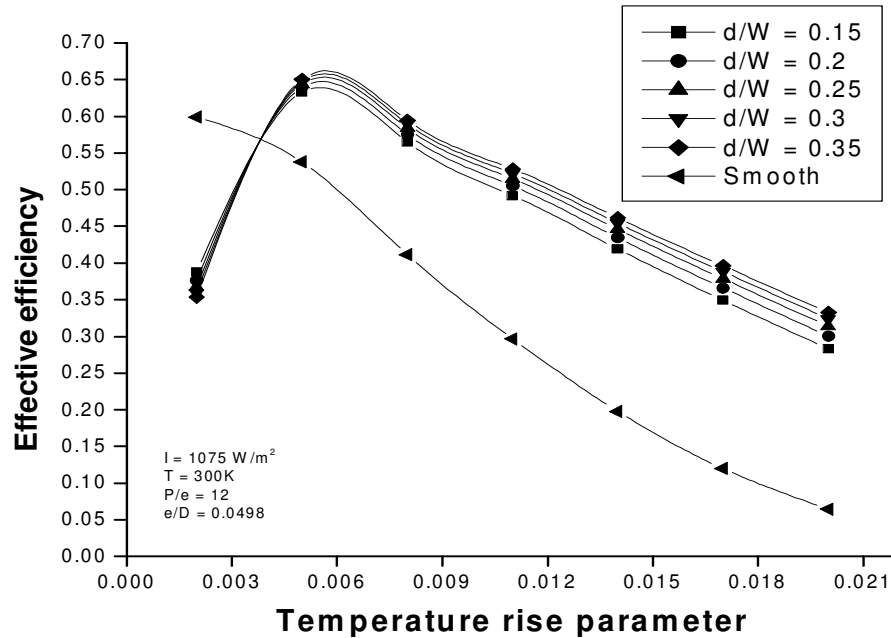


Figure 16. Effective efficiency Vs temperature rise parameter for $P/e= 12$ and $e/D=0.0498$.

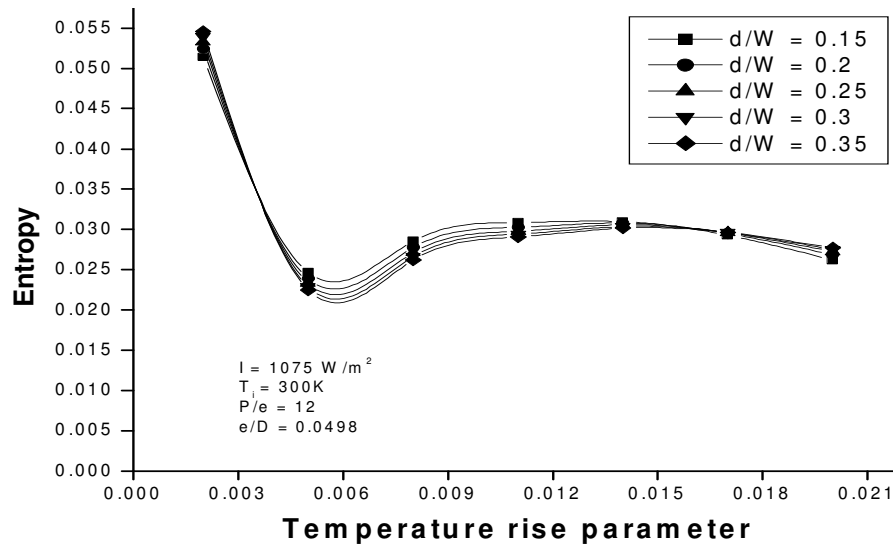


Figure 17. Entropy Vs temperature rise parameter for $P/e= 12$ and $e/D=0.0498$.

roughness pitch of 12 and relative gap position of 0.35. For the temperature rise parameter lower than 0.044 $\text{K/m}^2\text{W}$ relative roughness height of 0.0249 has minimum entropy generation number. For the temperature rise parameter between 0.044 to 0.016 $\text{K/m}^2\text{W}$ relative roughness height of 0.0498 has minimum entropy generation number. For the temperature rise parameter higher than 0.016 $\text{K/m}^2\text{W}$ relative roughness height of 0.0249 has minimum entropy generation number.

Figure 16 shows effective efficiency for five values of

relative gap position (d/W) for relative roughness pitch of 12 and relative roughness height (e/D) of 0.0498 and one for smooth absorber plate. For the temperature rise parameter lower than 0.038 $\text{K/m}^2\text{W}$ smooth absorber plate gives the best performance and relative gap position of 0.35 has minimum value of effective efficiency. For the temperature rise parameter higher than 0.038 $\text{K/m}^2\text{W}$ relative gap position of 0.35 has the best performance and smooth absorber plate has minimum value of effective efficiency. Figures 17 and 18 depict the effect of relative gap position on the entropy and entropy

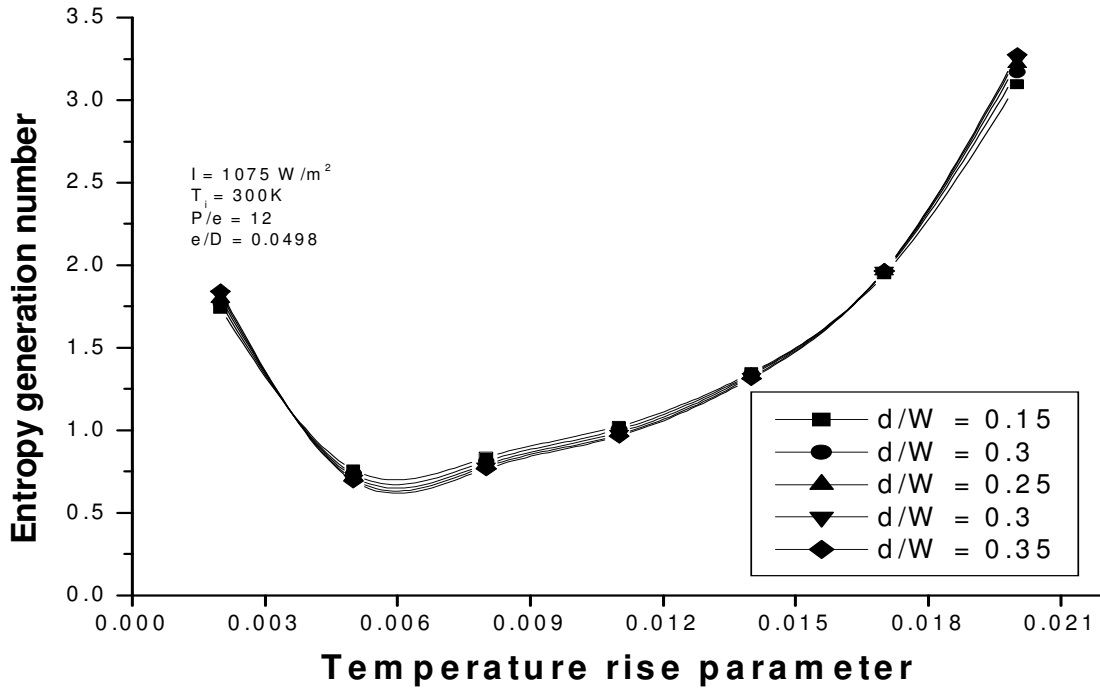


Figure 18. Entropy generation number Vs temperature rise parameter for $P/e= 12$ and $e/D=0.0498$. $\Delta T/I$.

generation number. For the temperature rise parameter lower than $0.038 \text{ K/m}^2\text{W}$ relative gap position of 0.15 has minimum value of entropy and entropy generation number. For the temperature rise parameter between 0.038 to $0.016 \text{ K/m}^2\text{W}$ relative gap position of 0.35 has minimum entropy and entropy generation number. For the temperature rise parameter higher than $0.016 \text{ K/m}^2\text{W}$ relative gap position of 0.15 has minimum value of entropy and entropy generation number.

CONCLUSIONS

The present analysis is undertaken with the objective of detailed study of effect of 60° inclined discrete rib artificial roughness on effective efficiency, entropy and entropy generation number. The effect of relative roughness pitch, relative roughness height and relative gap position on the effective efficiency, entropy and entropy generation number has been studied. It has been observed that for the temperature rise parameter lower than $0.038 \text{ K/m}^2\text{W}$ smooth absorber plate gives the higher effective efficiency.

But for the temperature rise parameter higher than $0.038 \text{ K/m}^2\text{W}$, 60° inclined discrete ribs arrangement provides the higher value of effective efficiency. The set of relative roughness pitch of 12, relative roughness height of 0.0498 and relative gap position of 0.35 shows the maximum effective efficiency and minimum entropy and entropy generation number for the temperature rise parameter nearly about $0.058 \text{ K/m}^2\text{W}$.

Nomenclatures

- A_p = Area of absorber plate, m^2 ; C = Conversion efficiency;
- C_p = Specific heat of air, J/Kg K ;
- D = Hydraulic diameter, m ;
- f = Friction factor;
- F_o = Heat removal factor;
- F_p = Collector efficiency factor;
- G_o = Mass velocity, Kg/sm^2 ;
- h = Average convective heat transfer coefficient, $\text{W/m}^2 \text{K}$;
- h_w = Wind convection coefficient, $\text{W/m}^2 \text{K}$;
- H = Duct depth, m ;
- I = Insolation, W/m^2 ;
- K = Thermal conductivity of air, W/m K ;
- k_i = Thermal conductivity of insulating material, W/m K ;
- L = Length of duct;
- L_1 = Height of collector casing, m ;
- \dot{m} = Mass flow rate of air, Kg/s ;
- N = number of glass cover;
- $N_{s,a}$ = Augmentation entropy generation number;
- Nu = Nusselt Number;
- P = Power consumed, W ;
- ΔP = Pressure drop through duct, Pa ;

p_r = Prudent number;
 q' = Heat transfer rate, W/m;
 Q_u = Useful heat gain;
 S = Tilt angle of collector as measured from horizontal;
 st = Stanton number;
 s'_{gen} = Entropy generation rate per unit duct length, W/Km;
 ds'_{gen} = Entropy generation rate, W/K;
 t_e = Thickness of side insulator, m;
 t_i = Thickness of bottom insulator, m;
 T_a = Ambient temperature of air, K;
 T_f = Mean bulk air temperature, K;
 T_i = Inlet temperature of air, K;
 T_o = Outlet temperature of air, K;
 T_p = Temperature of absorber plate, k;
 ΔT_m = Finite wall-bulk fluid temperature difference, K;
 ΔT = Temperature rise across the duct length, K;
 $\frac{\Delta T}{l}$ = Temperature rise parameter, K m²/W;
 U_b = Bottom loss coefficient, W/m² K;
 U_e = Edge loss coefficient, W/m² K;
 U_t = Top loss coefficient, W/m² K;
 U_L = Loss coefficient, W/m² K;
 V = Flow velocity;
 V_w = Wind velocity, m/s;
 W = Width of duct, m;

Greek symbols

σ = Stefan-Boltzman constant
 ρ = Density of air, Kg/m³
 μ = Dynamic viscosity, Kg/m s
 $\Gamma\alpha$ = Transmittance-absorptance product
 Ψ = Irreversibility distribution ratio
 α = Angle of attack of flow
 ϵ_p = Emittance of plate
 ϵ_g = Emittance of glass
 η_{eff} = Effective efficiency
 η_{th} = Thermal efficiency

REFERENCES

ASHRAE standard (1950). Methods of testing to determine the thermal performance of solar collectors. pp. 93-77.
 Bejan A (1982). Entropy generation through heat and fluid flow. New

York: Wiley-Intersci.Publi.
 Bragoria JS, Saini JS, Solanki SC (2002). Heat transfer co-efficient and friction factor correlation for rectangular solar air heater duct having transverse wedge shaped rib roughness on the absorber plate. Renewable Energy, 25: 341-369.
 Bhatti MS, Shah RK (1987). Turbulent and transition convective heat transfer in ducts. W. Wiley.
 Cavallero D, Tanda G (2002). An experimental investigation of forced convection heat transfer in channels with rib turbulators by means of liquid crystal thermography. Exp. Thermal Fluid Sci., 26:115-121.
 Cho HH, Kim YY, Rhee DH, Lee SY, Wu SJ (2003). The effect of gap position in discrete ribs on local heat/mass transfer in a square duct. J. Enhanced Heat Transfer, 10: 287-300.
 Cho HH, Wu SJ, Know HJ (2001). Local heat/mass transfer measurement in a rectangular duct with discrete rib. ASME J. Turbo Machinery, 122: 579-586.
 Cho HH, Wu SJ, Know HJ (2000). Local heat/mass transfer measurement in a rectangular duct with discrete rib. ASME J. Turbo machinery 122:579-586.
 Close DJ (1963). Solar air heaters for low and moderate temperature application. Solar Energy, 7: 117-124.
 Cortes A, Piacentini R (1990). Improvement of the efficiency of a bare solar collector by means of turbulence promoters. Appl. Energy, 36: 253-256.
 Gupta D, Solanki SC, Saini JS (1993). Heat and fluid flow in rectangular solar air heater ducts having transverse rib roughness on absorber plates. Solar Energy, 51: 31-37.
 Han JC, Zhang YM (1992). High performance heat transfer ducts with parallel, broken and V- shaped broken ribs. Int. J. Heat Mass Transfer, 35: 513-523.
 Jaurker AR, Saini JS, Gandhi BK (2006). Heat transfer and friction characteristics of rectangular solar air heater duct using rib-grooved artificial roughness. Solar Energy, 80: 895-907.
 Karmare SV, Tikekar AN (2007). Heat transfer and friction factor correlation for artificially roughened duct with metal grit ribs. Int. J. Heat and Mass Transfer, 50: 4342-4351.
 Karwa R, Solanki SC, Saini JS (1999). Heat transfer coefficient and friction factor correlations for the transitional flow regimes in rib-roughened rectangular duct. Int. J. Heat Mass Transfer, 42: 1597-1615.
 Kays WM (1996). Convective heat and mass transfer. McGraw Hill Inc., New York.
 Klien SA (1975). Calculation of flat plate loss coefficients. Solar Energy, 17: 79-80.
 Lau SC, McMillin RD, Han JC (1991). Heat transfer characteristics of turbulent flow in a square channel with angled rib. Trans. ASME J. Turbo- Machinery, 113: 367-374.
 Lau SC, McMillin RD, Han JC (1991). Turbulent heat transfer and friction in a square channel with discrete rib turbulators. Trans. ASME J. Turbomachinery, 113: 360-366.
 Layek A, Saini JS, Solanki SC (2007). Second law optimization of a solar air heater having chamfered rib-groove roughness on absorber plate. Renewable Energy, 32: 1967-1980.
 Momin AME, Sauna JS, Solanki SC (2002). Heat transfer and friction in solar air heater duct with V-shaped rib roughness on absorber plate. Int. J. Heat Mass Transfer, 45: 3383-3396.
 Prasad BN, Saini JS (1988). Effect of artificial roughness on heat transfer and friction factor in a solar air heater. Solar Energy, 41: 555-560.
 Saini RP, Saini JS (1997). Heat transfer and friction factor correlations for artificially roughened duct with expanded metal mesh as roughness element. Int. J. Heat Mass Transfer, 40: 973-986.
 Saini RP, Verma J (2008). Heat transfer and friction factor correlations for a duct having dimple-shape artificial roughness for solar air heater. Energy, 33: 1277-1287.
 Scott DF, Hewitt AL, MacDonald RA (2002). Calibration of an orifice meter. NACA Technical Memorandum 1940.
 Tanda C (2004). Heat transfer in rectangular channels with transverse and V-shaped broken ribs. Int. J. Heat Mass Transfer, 47: 229 243.
 Varun SRP, Singal SK (2008). Investigation of thermal performance of solar air heater having roughness elements as a combination of inclined and transverse ribs on the absorber plate. Renewable energy, 33: 1398-1405.